Journal of Computational Physics **171,** 95–114 (2001)
doi:10.1006/jcph.2001.6774, available online at http://www.idealibrary.com on IDEAL®

A Reversible Averaging Integrator for Multiple Time-Scale Dynamics[1]

Ben Leimkuhler* and Sebastian Reich†

*Department of Mathematics and Computer Science, University of Leicester, University Road, Leicester LE1 7RH, United Kingdom; and †Department of Mathematics, Imperial College, 180 Queen's Gate, London SW7 2BZ, United Kingdom
E-mail: B.Leimkuhler@mcs.le.ac.uk, S.Reich@ic.ac.uk

Received May 15, 2000; revised March 15, 2001

This paper describes a new reversible staggered time-stepping method for simulating long-term dynamics formulated on two or more time scales. By assuming a partition into fast and slow variables, it is possible to design an integrator that (1) averages the force acting on the slow variables over the fast motions and (2) resolves the fast variables on a finer time scale than the others. By breaking the harmonic interactions between slow and fast subsystems, this scheme formally avoids resonant instabilities and is stable to the slow-variable stability threshold. The method is described for Hamiltonian systems, but can also be adapted to certain types of non-Hamiltonian reversible systems.

Key Words: time-reversible multiple time-scale integrator; Verlet method; multirate methods.

CONTENTS

1. INTRODUCTION

The numerical integration of nonlinear Hamiltonian systems underpins much of modern computational science. In many applications such as molecular dynamics [7, 9], the systems

[1] This work was initiated while the authors were participants in the Foundations of Computational Mathematics program at the Mathematical Sciences Research Institute, in Berkeley, CA. Work at MSRI is supported by the National Science Foundation. Work by the first author was also supported by NSF DMS 9627330.

0021-9991/01 $35.00

are characterized by a multiplicity of time scales, generally meaning that a qualitatively important dynamic is manifest on a time interval much greater than the period of the fastest local oscillatory mode. In most cases, the long time-scale phenomena are of greatest interest, but it is difficult or impossible to model the slow and fast parts separately; although their local effect is weak, the fast components may—over a long period of time—make essential cumulative contributions to the evolution of any state.

The application of standard numerical integration methods is complicated by the presence of the fast modes. In many of the most important applications involving large-scale Hamiltonian models, it is found that explicit, low-order integrators, such as the Störmer–Verlet method, are the most effective. For a harmonic oscillator, the stability of a typical explicit numerical method is determined by a condition of the form $\Delta t\omega < D$, where Δt is the time step and ω is the frequency of the oscillator. For Störmer–Verlet, the constant is $D = 2$, meaning that at least three or four time steps are needed per period of the motion. A similar condition has been found to hold in nonlinear systems, where ω is the highest frequency present in the local linearization at any critical point. This stability restriction greatly limits the effectiveness of numerical integrators, and it is for this reason precisely that many interesting phenomena lie beyond the reach of simulation, even on the fastest computers available.

We distinguish two classes of multiscale phenomena. In the first class, the forces (or potential energies) separate additively into a hierarchy from weak to strong. Sometimes such a hierarchy can be artificially imposed on the system [10]. This additive decomposition can be used in the design of new methods, as in r-RESPA [12], hierarchical variable time stepping [10], the mollified impulse method [2], and the methods of [9]. In the second class of systems, the variables themselves are associated to different vibrational scales. Some models could fall into either category, but others do not, since it may not always be easy or natural to partition the variables as opposed to the forces. In some cases, an appropriate choice of coordinates may allow separation of the variables (see, e.g., [9] for an application in quantum–classical simulations).

In this article, we propose a "reversible averaging" (RA) method for the second category of multiscale mechanical models, based partly on the ideas of [2, 12]. Our method—which can be viewed as a generalization of Störmer-Verlet—does not require an additive decomposition of the potential. (Indeed, the method could as well be generalized to certain types of non-Hamiltonian time-reversible systems.) A key difference between our method and others that have been recently proposed is that we propagate the "fast" and "slow" variables by entirely different numerical and analytical processes, taking advantage of the available separation of scales. The method described here does not appear to have a natural interpretation as a "splitting method," a difference between our method and other approaches [2, 12] which appears to be key to avoiding instabilities. While the described approach is not symplectic, it does preserve the time-reversal symmetry of the flow of a mechanical system.

2. REVERSIBLE AVERAGING

Our method is based on the enormously popular Störmer–Verlet method applicable to Hamiltonians $H = \frac{1}{2}\boldsymbol{p}^T\boldsymbol{M}^{-1}\boldsymbol{p} + \boldsymbol{f}(\boldsymbol{q})$, where $\boldsymbol{M}$ is an $N \times N$ symmetric, positive-definite mass matrix and $f : \mathbb{R}^N \to \mathbb{R}$ is the potential energy. Viewed as a mapping of a point in phase space $(\boldsymbol{q}^0,\ \boldsymbol{p}^0)$ to a new point $(\boldsymbol{q}^1,\ \boldsymbol{p}^1)$, one step of the Störmer–Verlet method

divides into three parts: $\boldsymbol{p}^{1/2} = \boldsymbol{p}^0 - \frac{1}{2}\Delta t \nabla_{\boldsymbol{q}} f(\boldsymbol{q}^0)$, $\boldsymbol{q}^1 = \boldsymbol{q}^0 + \Delta t \boldsymbol{M}^{-1}\boldsymbol{p}^{1/2}$, and $\boldsymbol{p}^1 = \boldsymbol{p}^{1/2} - \frac{1}{2}\Delta t \nabla_{\boldsymbol{q}} f(\boldsymbol{q}^1)$. This method is explicit, time-reversible, symplectic, and second order in Δt.

Next consider a Hamiltonian of the form

$$\frac{1}{2}\boldsymbol{p}^T \boldsymbol{M}^{-1}\boldsymbol{p} + \frac{1}{2}\boldsymbol{\pi}^T \hat{\boldsymbol{M}}^{-1}\boldsymbol{\pi} + f(\boldsymbol{q}, \boldsymbol{\theta}), \tag{1}$$

where $\boldsymbol{q}$ and $\boldsymbol{p}$ are the "slow variables," and, due either to the structure of the potential energy or to the variation in masses, the variables $\boldsymbol{\theta}$ and the momenta $\boldsymbol{\pi}$ may be regarded as "fast variables." Our goal is to deffne a symmetric generalization of Störmer–Verlet which incorporates an averaging on the fast degrees of freedom and, importantly, a more accurate integration of those variables.

The differential equations corresponding to (1) take the form

$$\frac{d}{dt}\boldsymbol{q} = \boldsymbol{M}^{-1}\boldsymbol{p}, \qquad \frac{d}{dt}\boldsymbol{p} = -\nabla_{\boldsymbol{q}} f(\boldsymbol{q}, \boldsymbol{\theta}), \tag{2}$$

$$\frac{d}{dt}\boldsymbol{\theta} = \hat{\boldsymbol{M}}^{-1}\boldsymbol{\pi}, \qquad \frac{d}{dt}\boldsymbol{\pi} = -\nabla_{\boldsymbol{\theta}} f(\boldsymbol{q}, \boldsymbol{\theta}). \tag{3}$$

We term (2) the "slow" subsystem and (3) the "fast" subsystem.

The way in which the fast variables are propagated in our algorithm depends on the problem. Assuming the evolution of $\boldsymbol{q}$ to be known (described by $\boldsymbol{q} = \hat{\boldsymbol{q}}(t)$), observe that the fast variables can be viewed as the solution of a reduced time-dependent nonautonomous Hamiltonian $\hat{H}_{[\hat{\boldsymbol{q}}(t)]} = \frac{1}{2}\boldsymbol{\pi}^T \hat{\boldsymbol{M}}^{-1}\boldsymbol{\pi} + f(\hat{\boldsymbol{q}}(t), \boldsymbol{\theta})$. Given the slow evolution, it may, in certain cases, be possible to recover the fast variables exactly, but in typical situations, the computation would be better effected by a numerical method. If the fast subsystem is substantially smaller than the slow one (as it is in many applications), then it is reasonable to think of solving this system more accurately than the slow one; thus, for example, we might introduce a reduction factor $1/M$ in the size of the time step used for the recovery of the averages and propagation of the fast variables compared to the size of the outer time step Δt.

To illustrate the potential speedup from this method, consider the extreme scenario in which there are N_S slow variables and only one fast variable, and assume that all variables are coupled, so that the work to evaluate forces is proportional to $N_S^2/2$. On the other hand, the work required to compute interactions between the fast variable and the slow variables is proportional to N_S. If N_S is large and the partitioning method can achieve even a small increase in the stability of the method with a value of $M \ll N_S$, then the savings could clearly be quite dramatic. These benefits would extend to systems with a few fast degrees of freedom, or to systems where the fast force calculation is for other reasons much less costly than the computation of the slow forces.

We next present the details of the method in mathematical form.

ALGORITHM 1 (Reversible Averaging Method for Two Time Scales).
Given: $\boldsymbol{q}^0, \boldsymbol{p}^0, \boldsymbol{\theta}^0, \boldsymbol{\pi}^0$.

1. Compute the solution $(\boldsymbol{\theta}_+(t), \boldsymbol{\pi}_+(t))$ for Hamiltonian $\hat{H}_{[\boldsymbol{q}^0]}$, starting from $(\boldsymbol{\theta}^0, \boldsymbol{\pi}^0)$ at $t = 0$.

2. Slow variable half-step. Compute a time-averaged force

$$\bar{\boldsymbol{F}}_+ = -\frac{1}{b\Delta t}\int_0^{b\Delta t} \nabla_q f(q^0, \theta_+(t))\, dt,$$

then apply the Störmer–Verlet method to compute the position using this force:

$$\boldsymbol{p}^{1/2} = \boldsymbol{p}^0 + \frac{\Delta t}{2}\bar{\boldsymbol{F}}_+,$$
$$\boldsymbol{q}^1 = \boldsymbol{q}^0 + \Delta t \boldsymbol{M}^{-1}\boldsymbol{p}^{1/2}.$$

3. Compute the solution $(\boldsymbol{\theta}_*(t), \boldsymbol{\pi}_*(t))$ of the t-dependent Hamiltonian $\hat{H}_{[\hat{\boldsymbol{q}}(t)]}$, starting from $(\boldsymbol{\theta}^0, \boldsymbol{\pi}^0)$ at $t = 0$, with $\hat{\boldsymbol{q}}(t)$ moved along a linear path: $\hat{\boldsymbol{q}}(t) = \boldsymbol{q}^0 + t\boldsymbol{M}^{-1}\boldsymbol{p}^{1/2}$. Next set

$$\boldsymbol{\theta}^1 = \boldsymbol{\theta}_*(\Delta t),$$
$$\boldsymbol{\pi}^1 = \boldsymbol{\pi}_*(\Delta t).$$

4. Integrate the fast variable $\boldsymbol{\theta}_-(t)$, backward in time, holding the slow variables fixed at $\boldsymbol{q}^1$.

5. Slow momentum update. Compute

$$\bar{\boldsymbol{F}}_- = -\frac{1}{b\Delta t}\int_{(1-b)\Delta t}^{\Delta t} \nabla_q f(q^1, \theta_-(t))\, dt.$$

Then update the momentum:

$$\boldsymbol{p}^1 = \boldsymbol{p}^{1/2} + \frac{\Delta t}{2}\bar{\boldsymbol{F}}_-.$$

An alternative would be to hold $\boldsymbol{q}$ fixed at its half-step value during the fast propagation step (Step 3). The method would then be similar to a scheme given in [12]. To refer to this method in the sequel, we will call the resulting modified scheme (with $\boldsymbol{q}$ fixed at $\boldsymbol{q}^{1/2}$ during Step 3) *RA-0*, and the method given above (with linear movement of $\boldsymbol{q}$ during the fast propagation) *RA-1*.

Note that an appropriate scheme must be used to compute the finite time average of $\nabla_{\boldsymbol{q}} f(\hat{\boldsymbol{q}}, \boldsymbol{\theta}(t))$. The precise way in which this is carried out may be very important for the success or failure of the method in applications. If the force acting on the slow particles is linear in the fast variables $\boldsymbol{\theta}$, then the average to be computed for the slow momentum updates becomes

$$\langle \nabla_{\boldsymbol{q}} f(\hat{\boldsymbol{q}}, \boldsymbol{\theta})\rangle = \nabla_{\boldsymbol{q}} f(\boldsymbol{q}, \langle\boldsymbol{\theta}\rangle).$$

This property eliminates much of cost of averaging. The same simplified averaging may be used whenever $\boldsymbol{\theta} - \langle\boldsymbol{\theta}\rangle$ is sufficiently small. This issue is clarified in the following section for several examples. In experiments described later, we found no advantage to averaging outside the interval defined by the outer time step ($b > 1$).

To see that Algorithm 1 is time-reversible, one needs to check that the inverse time-step map with Δt replaced by $-\Delta t$ is the same as the original map. To develop the inverse map,

we work backward from the last step of the method. Given $(\boldsymbol{q}^1, \boldsymbol{p}^1)$, one must first compute the averaged force $\bar{\boldsymbol{F}}_-$, before $\boldsymbol{p}^{1/2}$ can be computed. The backward averaging would be the same as the forward averaging in Step 2 if we were to make the substitutions $\Delta t \to -\Delta t$ and $\boldsymbol{q}^1 \to \boldsymbol{q}^0$. The computation of $\boldsymbol{p}^{1/2}$ and $\boldsymbol{q}^{1/2}$ by inverting Steps 6 and 4 is then analogous to Step 2 of the algorithm with the same substitutions and $\boldsymbol{p}^1 \to \boldsymbol{p}^0$. Finally Step 3 is itself symmetric since it is the flow of a reversible Hamiltonian system. Denoting the time-step map by $\Phi_{\Delta t}$, we conclude $\Phi_{-\Delta t}^{-1} = \Phi_{\Delta t}$,

The usual property of time-reversal symmetry, i.e., a reversing symmetry with respect to the involution $\mathcal{R} : (\boldsymbol{q}, \boldsymbol{p}) \to (\boldsymbol{q}, -\boldsymbol{p})$, then follows, since it is easy to verify that

$$\mathcal{R} \circ \Phi_{\Delta t} = \Phi_{-\Delta t} \circ \mathcal{R},$$

implying

$$\mathcal{R} \circ \Phi_{\Delta t} \circ \mathcal{R} \circ \Phi_{\Delta t} = \mathrm{Id},$$

with Id the identity map.

The second-order convergence follows from (1) the one-step character of the method, (2) its obvious consistency, and (3) its symmetry [3].

In Appendix A, the method of Algorithm 1 is extended to treat a multiplicity of time scales, using successively smaller time steps to handle the faster sets of variables.

3. APPLICATIONS

Before continuing with analysis and numerical experiments, we mention several illustrative classes of problems that could directly benefit from the use of the reversible averaging integrator.

First, consider an example from gravitation: the case of a "slow-moving" star field with a handful of fast binaries. We may view the positions and momenta of the binaries as the "fast variables." To make the method efficient, we expect to replace the slow force average over the fast motion by the slow force evaluated at the average fast position, which should be reasonable under the assumption of no close approaches of the binaries to the other stars.

Examples of a quite difererent nature involving a small mass arise in the context of various quantum–classical models such as the Car–Parrinello method [1] and in simplified approaches such as one encounters in polarization studies [11]. Here the "fast" variables describe—perhaps crudely—the electronic structure, and the slow variables are associated to the locations of the atomic nuclei. Such models typically involve small fictitious mass parameters which keep the associated kinetic energy of the electronic degrees of freedom close to zero. Although in standard Car–Parinello approaches the fast forces dominate the computational cost, we believe that some of the more simplified models could benefit from the clear separation between the fast electronic degrees of freedoms and the slow classical degrees of freedom, through the use of our averaging approach.

As a third example, we consider quantum–classical molecular dynamics [4, 8]. We are especially interested in the case of very large systems, where a full nonadiabatic–quantum mechanical approximation is only needed for a small portion of the system such as the quantum–mechanical transition of a hydrogen atom. In the simplified case of a single

quantum degree of freedom, the quantum–classical energy takes the form

$$H(\boldsymbol{p}, \boldsymbol{q}, \psi) = \frac{1}{2}\boldsymbol{p}^T \boldsymbol{M}^{-1}\boldsymbol{p} + \langle \psi, \mathbf{T}\psi \rangle + \langle \psi, \mathbf{V}(\boldsymbol{q})\psi \rangle + U_{cl}(\boldsymbol{q}),$$

where $\mathbf{T}$ and $\mathbf{V}(\boldsymbol{q})$ are the spatial discretizations of the associated quantum Hamiltonian operator $H = T + V(\boldsymbol{q})$, and we have used $\langle .\,, .\rangle$ to indicate the L_2 inner product. The method of Section 2 can be implemented with minor adjustments. Specifically, we freeze $\boldsymbol{q}$ and $\boldsymbol{p}$ and obtain $\bar{\psi}(t)$ by solving a Schrödinger equation. We compute the average Hellmann–Feynman force acting on the classical coordinates from

$$-\frac{1}{t}\int_0^t \langle \bar{\psi}(t), \nabla_{\boldsymbol{q}} \mathbf{V}(\boldsymbol{q}_n)\bar{\psi}(t)\rangle \, dt,$$

or the method suggested in [4]. Note that, due to the structure of the system, only a single evaluation of the classical forces—$\nabla_{\boldsymbol{q}} U_{cl}(\boldsymbol{q})$ and the matrix operator $\nabla_{\boldsymbol{q}}\mathbf{V}(\boldsymbol{q}_n)$ is required per time step. The averaging over the quantum degree of freedom should be carried out accurately to obtain the correct effective Hellmann–Feynman force. The same holds true for the propagation of the fast quantum degrees of freedom which should ensure the evolution of correct quantum occupation numbers. Here a linear propagation of the classical degrees of freedom (variant RA-1) should provide a significant improvement over variant RA-0.

4. STABILITY

In [2], for linear or near-linear problems, instabilities were found to occur at certain isolated values of the step size; they are artifacts of introducing resonance with the fast modes of the problem into the discretized slow dynamics, and are therefore termed "step size resonances."

Our methods are also potentially subject to such resonances, and we study them in this section for a linear model problem. Whereas the RA-0 method is found to have resonances near $\Delta t = 2k\pi/\omega$, $k = 1, 2, \ldots$, it is shown that the RA-1 method *does not have any resonances*, although there are potentially harmful *near-resonances.* In the numerical experiments, we indicate how these step size resonances and near-resonances manifest themselves in nonlinear models.

For the purpose of understanding the resonances, let us introduce a linear Hamiltonian system with energy

$$H = \frac{1}{2}p^2 + \frac{1}{2\mu}\pi^2 + \frac{1}{2}q^2 + \frac{1}{2}k(q-\theta)^2,$$

where μ and k are parameters. For this analysis, we will take $k = \omega = 1/\mu$. The linear system has two sinusoidal components with frequencies ω_+, ω_-:

$$\omega_\pm = \left(\frac{\eta \pm \sqrt{\eta^2 - 4\omega^2}}{2}\right)^{1/2}, \quad \eta = \omega^2 + \omega + 1.$$

For large ω, we have

$$\omega_+ \sim (1 + \omega + \omega^2)^{1/2} \sim \omega,$$

and

$$\omega_- \sim \left(\frac{\omega^2}{1+\omega+\omega^2}\right)^{1/2} \sim 1.$$

and we therefore term ω as the frequency of fast oscillation.

The solution behavior becomes even more apparent on going to the transformed coordinates $q_1 := q$ and $q_2 := \theta - q$. The corresponding canonical momenta are given by $p = p_1 - p_2$ and $\pi = p_2$. Thus the transformed Hamiltonian is

$$H = \frac{1}{2}(p_1 - p_2)^2 + \frac{1}{2\mu}p_2^2 + \frac{1}{2}q_1^2 + \frac{1}{2}kq_2^2.$$

Take $k = \omega = 1/\mu \gg 1$. Then the system is well separated into a fast and slow component, implying that the energy

$$E_{\text{fast}} = \frac{\omega}{2}\left(p_2^2 + q_2^2\right)$$

of the fast degree of freedom is almost constant along solutions. Furthermore, provided the energy H is bounded, the variable p_2 is of order $\omega^{-1/2}$ and the energy $E_{\text{slow}} := H - E_{\text{fast}}$ satisfies

$$E_{\text{slow}} = \frac{1}{2}\left(p_1^2 + q_1^2\right) + \mathcal{O}\left(\omega^{-1/2}\right).$$

Since

$$\theta = q_1 + q_2 = q + \mathcal{O}\left(\omega^{-1/2}\right),$$

the variable θ follows q adiabatically at a distance of order $\omega^{-1/2}$.

We consider the application of the RA-0 or RA-1 method with exact resolution of the fast variables. Applying the method to the linear model problem, we obtain a linear map of $\mathbb{R}^4$, the numerical propagator, which is a function of ω and Δt. An eigenvalue analysis can then be used to examine the crossing points of eigenvalues which can give rise to resonant behavior.

4.1. *Construction of the Discrete Propagator*

The solution of the linear system $\dot{\theta} = \omega\pi$; $\dot{\pi} = -\omega\theta + \gamma + t\delta$ with initial conditions θ^0 and π^0 is

$$\theta(t) = C_1\hat{c}(t) + C_2\hat{s}(t) + (\gamma + t\delta)/\omega; \qquad \pi(t) = -C_1\hat{s}(t) + C_2\hat{c}(t) + \delta/\omega^2,$$

where $\hat{c}(t) = \cos(\omega t)$, $\hat{s}(t) = \sin(\omega t)$. Also we write $\hat{c} = \hat{c}(\Delta t)$, $\hat{s} = \hat{s}(\Delta t)$.

Force averaging and average value plugged into the force are the same for the linear problem. At the first step of RA-1, we average the fast position variable forward on $[0, b\Delta t]$, after computing with $q = q^0$; hence we obtain

$$\bar{\theta} = (\theta^0 - q^0)S + \pi^0 C + q^0,$$

where

$$S = \sin(b\omega\Delta t)/(b\omega\Delta t), \qquad C = (1-\cos(b\omega\Delta t))/(b\omega\Delta t).$$

The next step is propagation of the slow variables for a half-step,

$$\begin{aligned} q^{1/2} &= q^0 + \frac{1}{2}\Delta t p^{1/2} \\ p^{1/2} &= p^0 - \frac{1}{2}\Delta t(q^0 + \omega(q^0 - \bar{\theta})) \\ &= p^0 - \frac{1}{2}\Delta t(q^0 - \omega((\theta^0 - q^0)S + \pi^0 C)). \end{aligned}$$

We can already write the formula for q^1:

$$q^1 = q^0 + \Delta t p^{1/2}.$$

Now we propagate the fast variables. This step is different for RA-0 or RA-1. For RA-0 we have

$$\begin{aligned} \theta^1 &= C_1\hat{c} + C_2\hat{s} + q^{1/2}, \\ \pi^1 &= -C_1\hat{s} + C_2\hat{c}, \end{aligned}$$

with constants

$$C_1 = \theta^0 - q^{1/2}, \qquad C_2 = \pi^0,$$

whereas, for RA-1, we have

$$\begin{aligned} \theta^1 &= C_1\hat{c} + C_2\hat{s} + q^1, \\ \pi^1 &= -C_1\hat{s} + C_2\hat{c} + \frac{p^{1/2}}{\omega}, \end{aligned}$$

with

$$C_1 = \theta^0 - q^0, \qquad C_2 = \pi^0 - \frac{p^{1/2}}{\omega}.$$

In the next step of the algorithm, we solve the fast system backward, then average and substitute to compute the update of the slow momentum. However, the method is symmetric, so we must have

$$p^1 = p^{1/2} - \frac{1}{2}\Delta t(q^1 - \omega((\theta^1 - q^1)S - \pi^1 C)).$$

The 4×4 matrix propagators for each of the two methods are now easily formulated. These expressions are given in Appendix B. The following properties of these matrices ($\mathcal{M}(\Delta t)$ and $\mathcal{N}(\Delta t)$, respectively, for RA-0 and RA-1) have been verified for step sizes below the slow-variable stability threshold: (1) they are third-order approximations of the exact

propagator, (2) they satisfy the symmetry property $\mathcal{M}(-\Delta t)^{-1} = \mathcal{M}(\Delta t), \mathcal{N}(-\Delta t)^{-1} = \mathcal{N}(\Delta t)$, and (3) they are reversible with respect to the involution

$$\mathcal{R} = \begin{bmatrix} 1 & 0 & 0 & 0 \\ 0 & 1 & 0 & 0 \\ 0 & 0 & -1 & 0 \\ 0 & 0 & 0 & -1 \end{bmatrix},$$

meaning that

$$\mathcal{R}\mathcal{M}\mathcal{R}\mathcal{M} = I,$$

with a similar equation for $\mathcal{N}$. As a consequence of the reversing symmetry property and the fact that the matrix is real, the following properties hold for the spectrum,

1. If $\lambda \in \sigma(\mathcal{M})$, then $1/\lambda \in \sigma(\mathcal{M})$,
2. If $\lambda \in \sigma(\mathcal{M})$, then $\bar{\lambda} \in \sigma(\mathcal{M})$,

with similar formulas for $\mathcal{N}$. For example, one possibility for the spectrum is four distinct eigenvalues—$\lambda_1, \lambda_2, \bar{\lambda}_1, \bar{\lambda}_2$—all on the unit circle S. Another possibility is to have an eigenvalue λ off the unit circle, together with its reciprocal and the conjugates of those two numbers.

4.2. *Stability, Slow and Fast Modes, Crossings, and Resonance*

Viewed as functions of the parameter Δt, we can think of the eigenvalues as describing curves on or near the unit cylinder $S \times \mathbb{R}_+$ where height is measured by Δt. Such curves are shown in Fig. 1 for the RA-0 method. Four curves are shown, one for each eigenvalue. As the time step parameter is increased at $\Delta t = 0$, the four eigenvalues separate from unity. Observe that two eigenvalues move around the circumference of the cylinder; the other two eigenvalues slowly separate near one.

Each of the conjugate eigenvalue pairs of the propagator can be viewed as an approximation to either the fast or the slow mode of the continuous problem. Exponential instability arises when the eigenvalues move outside the unit circle. Resonant instability is associated to degeneracy of the eigenspace of the problem, a necessary condition for which is crossing of eigenvalues. However, not all eigenvalue crossings cause problems for the discrete dynamics, and near-crossings can also cause problems in the numerical simulation. A better indicator of resonance than crossings is the largest eigenvalue condition number, defined as the reciprocal of the cosine of the angle between the left and right eigenvectors associated to an eigenvalue; near points of degeneracy of the matrix, the eigenvalue condition numbers tend to infinity.

In Fig. 2, the real and imaginary parts of the eigenvalues of the matrix $\mathcal{M}$ (RA-0) are shown for the step size interval [0.001, 0.041] and the imaginary parts on subintervals near the first two crossings. The large interval figures are visually identical for the RA-1 method, but there are significant differences in the detail near the crossing points; these are shown in Fig. 3. As the step size is increased, the slow eigenvalue pair moves monotonically to the left while the fast eigenvalues repeatedly orbit the unit circle. For both the RA-0 and RA-1 methods, crossings of the fast eigenvalues are found in the vicinity of the points $\pi/\omega, 2\pi\omega, 3\pi\omega$, etc., while the slow eigenvalue/fast eigenvalue pairs approach very near to even multiples of π/ω.

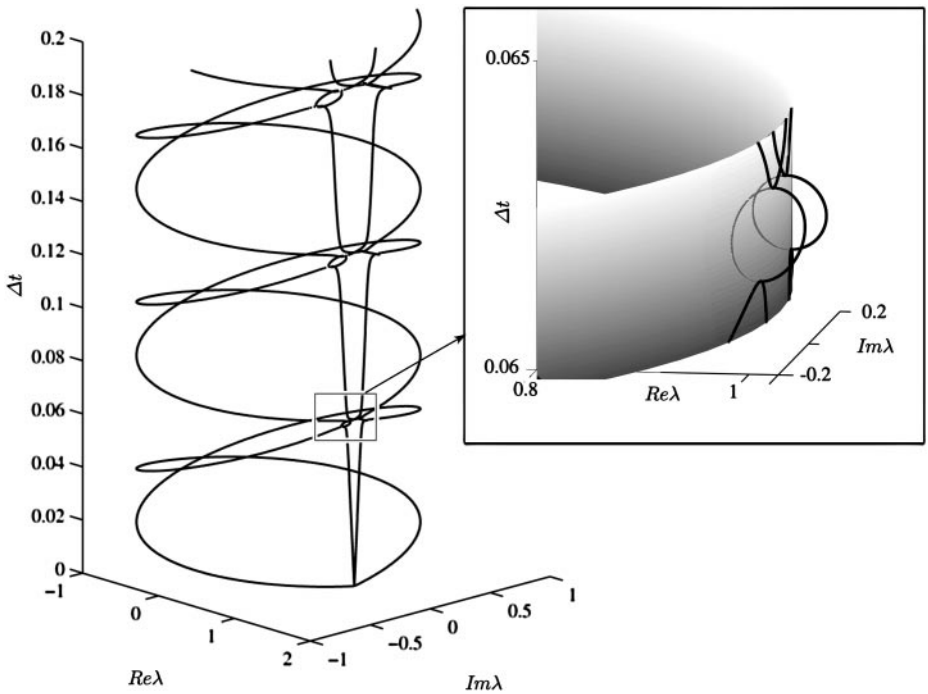

FIG. 1. Eigenvalues of RA-0, $\omega = 100$. The eigenvalues of can be viewed as curves near the unit cylinder with height parameterized by the timestep Δt; instabilities can occur near eigenvalue crossings, either because the eigenvalues leave the cylinder or because of degeneracy of the eigenspace.

Evaluating the matrices $\mathcal{M}$ and $\mathcal{N}$ at each of the fast–fast crossings is straightforward. We now take a closer look at the structure of these propagators. The real Schur decomposition of a matrix A is written $A = QTQ^T$, with Q orthogonal and T block upper triangular; the properties of the powers of the matrix A can be understood in terms of the associated

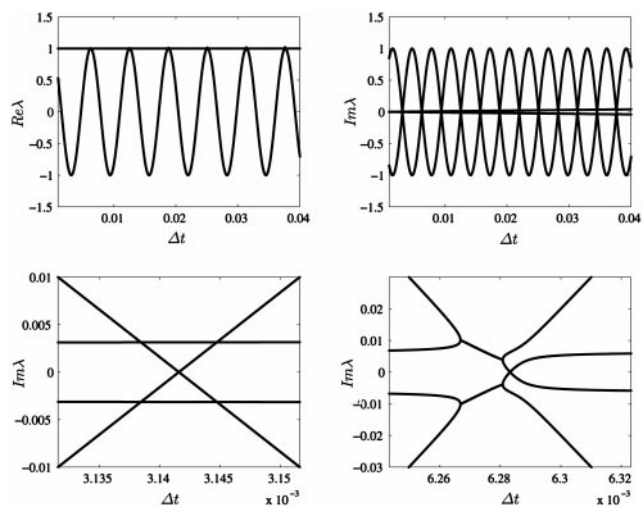

FIG. 2. RA-0 eigenvalues as function of the step size, $\omega = 1000$. Clockwise from upper left, real parts of the eigenvalues on a long interval in the step size, imaginary parts of the eigenvalues on a long interval, imaginary parts, short interval near an even multiple of π/ω, short interval near an odd multiple of π/ω.

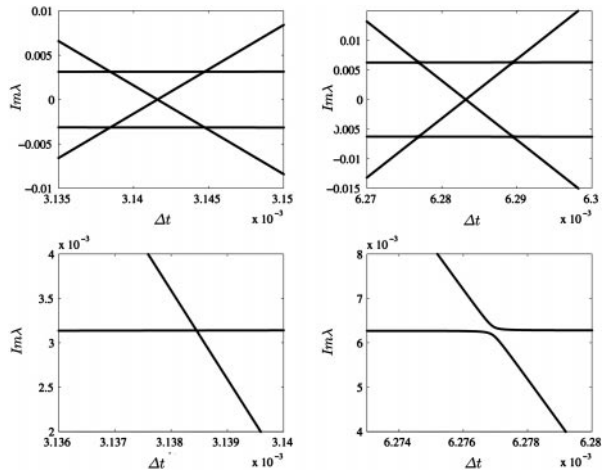

FIG. 3. Imaginary parts of eigenvalues, RA-1, near first two multiples of $\pi, \omega = 1000$. Note the close approaches ("avoided crossings") of eigenvalues which imply that instability (resonant or exponential) is not encountered.

properties of the matrix T. After a suitable coordinate transformation, we have the 2×2 block decomposition

$$T = \begin{bmatrix} S & C \\ 0 & F \end{bmatrix},$$

where S corresponds to the "slow" variables, and C and F act on the fast variables. At the odd multiples of π, we have, for both RA-0 and RA-1, $F = -I, C = O(1)$, and S is a representation of the discrete propagator corresponding to the Störmer–Verlet method applied to just the slow modes, which is a stable matrix (separated eigenvalues on the unit circle) for $\omega_- \Delta t < 2$. We note that

$$T^N = \begin{bmatrix} S^N & B_N C \\ 0 & (-1)^{N+1} I \end{bmatrix},$$

where

$$B_N = (-1)^{N-1} \sum_{i=0}^{N-1} (-S)^i = (-1)^{N-1} (I + S^N)(I + S)^{-1}.$$

Clearly S^N and also B_N are bounded. Moreover, this means that T is power bounded.

At the even multiples of π/ω, the picture is similar except that (1) $F = I$, (2) for RA-0, C turns out to be $O(\Delta t)$, while (3) for RA-1, $C = 0$; the situation with respect to fast–fast resonances is only improved.

We next turn our attention to the potentially more serious case of slow–fast crossings, which occur at two points near each even multiple of π/ω. We first note that there is an instability in RA-0 *just to the left of the even multiples of* π/ω. The reader is referred to Fig. 1 for an illustration of the situation. Here, two slow–fast crossings are observed. These points are associated to reversible Hopf bifurcations [6] (the reversible analogue of symplectic Krein-crunch bifurcations), in which two unit-modulus eigenvalues (and their

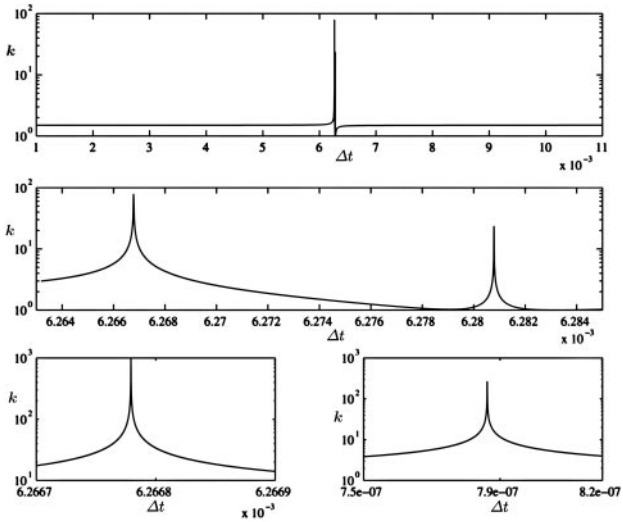

FIG. 4. Eigenvalue condition numbers for RA-0, $\omega = 1000$.

complex conjugates) of a reversible matrix coalesce and leave the unit circle. In fact there is a narrow band between the two crossings where a pair of eigenvalues moves off the unit circle.

On the other hand, the slow and fast eigenvalues for RA-1 come close, but *do not cross*! (See Fig. 3.) This remarkable feature of the RA-1 method is the likely explanation for its marked superiority to RA-0 in large stepsize integration, as we will see in the next section. For this reason, *the RA-1 method does not exhibit any resonant or exponential instability below the stability threshold for the Verlet method applied to the slow subsystem*. The RA-1 propagator is power bounded regardless of stepsize (up to the slow variable stability threshold), although that attained bound may be relatively large in the vicinity of near-crossings of the eigenvalues (at two points in the vicinity of even multiples of π/ω).

The eigenvalue condition numbers reflect these observations. Let κ represent the largest of these for any given value of the stepsize, for Δt in the interval [0.001, 0.011]. In Fig. 4, κ is graphed against the stepsize for the RA-0. We see that the eigenvalue condition number is moderate for most of the interval considered, but becomes quite large just to the left of $2\pi/\omega$. Close-ups show that there are two sharp peaks, well correlated to the eigenvalue crossings discussed above.

The situation for the RA-1 method is quite different. Corresponding graphs of κ are shown in Fig. 5. Only a relatively mild increase in condition number can be seen at or near the points where the fast and slow eigenvalues of $\mathcal{N}$ have close approaches on either side of $2\pi/\omega$.

5. NUMERICAL EXPERIMENT

We implemented the two-scale RA method with numerical averaging of the fast variables using the Störmer–Verlet method. Our aim in this experiment was to show that the

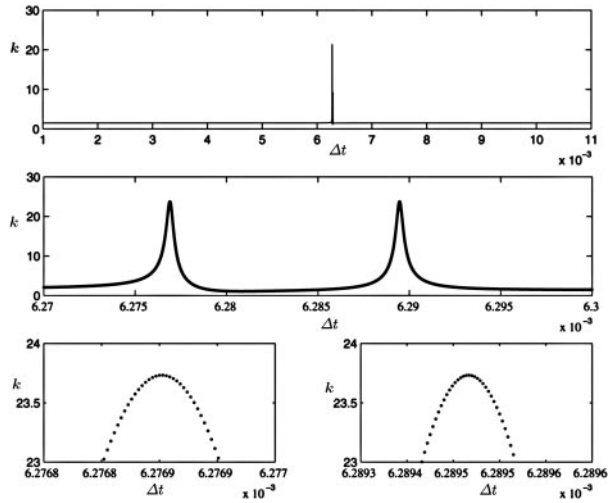

FIG. 5. Eigenvalue condition numbers for RA-1, $\omega = 1000$.

reversible averaging method performs stably in the large step size regime, thus we have neglected performance and efficiency issues and concentrated only on demonstrating the convergence and accuracy of the method at stepsizes at or above the Störmer–Verlet stability limit.

We simulated a pair of masses moving in the plane in the potential

$$V(\boldsymbol{q}, \boldsymbol{\theta}) = \frac{1}{2}(|\boldsymbol{q}|) - 1)^2 + \frac{1}{2}\kappa|\boldsymbol{q} - \boldsymbol{\theta}|^2.$$

Physically, $\boldsymbol{q}$ represents the position of a massive particle attached through a soft spring with unit rest length to a fixed point at the origin; a second moving particle (at position $\boldsymbol{\theta}$) is connected to the first by a harmonic spring with coefficient κ. A unit mass is assumed for the first bob, while the second is treated as a parameter μ. If κ is large and/or μ is small, we have a two-scale dynamical system. This can be seen by going to transformed coordinates $(\boldsymbol{q}_1, \boldsymbol{q}_2, \boldsymbol{p}_1, \boldsymbol{p}_2)$ defined by

$$\begin{pmatrix} \boldsymbol{q}_1 \\ \boldsymbol{q}_2 \end{pmatrix} = \begin{pmatrix} I & 0 \\ -I & I \end{pmatrix} \begin{pmatrix} \boldsymbol{q} \\ \boldsymbol{\theta} \end{pmatrix} \quad \text{and} \quad \begin{pmatrix} \boldsymbol{p} \\ \boldsymbol{\pi} \end{pmatrix} = \begin{pmatrix} I & -I \\ 0 & I \end{pmatrix} \begin{pmatrix} \boldsymbol{p}_1 \\ \boldsymbol{p}_2 \end{pmatrix}.$$

The corresponding tranformed Hamiltonian is

$$H = \frac{1}{2}|\boldsymbol{p}_1 - \boldsymbol{p}_2|^2 + \frac{\omega}{2}|\boldsymbol{p}_2|^2 + \frac{1}{2}(|\boldsymbol{q}_1| - 1)^2 + \frac{\omega}{2}|\boldsymbol{q}_2|^2.$$

The energy

$$E_{\text{fast}} = \frac{\omega}{2}(|\boldsymbol{p}_2|^2 + |\boldsymbol{q}_2|^2)$$

of the fast degrees of motion is an adiabatic invariant [1] for $\omega \gg 1$ and, hence, is almost preserved along solutions. Thus the slow degrees of freedom $(\boldsymbol{q}_1, \boldsymbol{p}_1)$ stay close to the energy surface

$$E_{\text{slow}} = \frac{1}{2}\,|\boldsymbol{p}_1|^2 + \frac{1}{2}(|\boldsymbol{q}_1| - 1)^2.$$

Furthermore, since

$$\boldsymbol{\theta} = \boldsymbol{q}_1 + \boldsymbol{q}_2 = \boldsymbol{q} + \mathcal{O}\big(\omega^{-1/2}\big),$$

the fast variable $\boldsymbol{\theta}$ follows $\boldsymbol{q}$ adiabatically at a small distance of order $\omega^{-1/2}$.

A related—though more complex—model in molecular dynamics would be the classical water molecule which has a heavy central oxygen and two lightweight hydrogens connected to the oxygen by what are effectively stiff springs (in addition to other interaction forces).

We chose $\kappa = 1000$ and $\mu = 0.001$, so that we had a strong fast mode (with high frequency $\omega = \sqrt{\kappa/\mu} = 1000$), distinguishing two important cases for the initial conditions. In data set A, we took $\boldsymbol{q}^0 = (1, 0)$, $\boldsymbol{\theta}^0 = (1, 0)$, $\boldsymbol{p}^0 = (0, 1)$, and $\boldsymbol{\pi}^0 = (0, 0.05)$, so that a substantial fast energy is present at the initial point. The trajectory for these initial data is shown in Fig. 6. In data set B, the initial conditions were the same as in dataset A, except $\boldsymbol{\pi}^0 = (0, 0)$; in this case, all the initial energy is present in the slow components.

When the system is solved with the Störmer–Verlet method, the stepsize is restricted approximately according to the condition

$$\Delta t \sqrt{\kappa/\mu} \leq 2.$$

For example, when $\kappa = 1000$ and $\mu = 0.001$, as in our experiments, the theoretical condition is $\Delta t < 0.002$. In our experiments, and for both data sets A and B, the Störmer–Verlet method indeed became unbounded at $\Delta t = 0.002$.

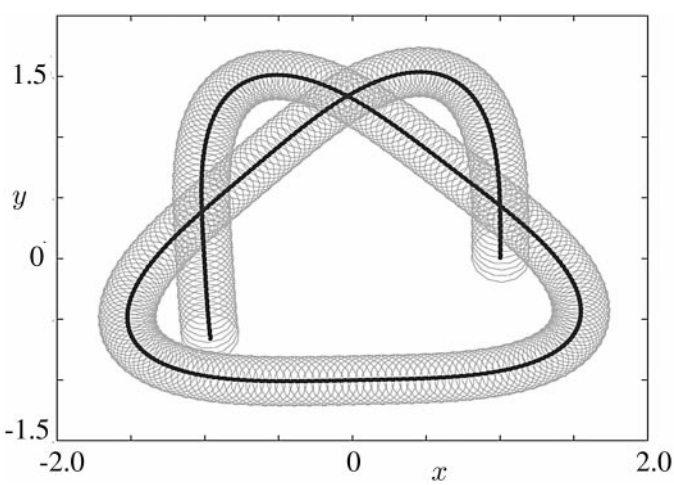

FIG. 6. Trajectories of the two-particle spring–mass system, showing the heavy particle motion (bold) and the oscillations of the light particle (light).

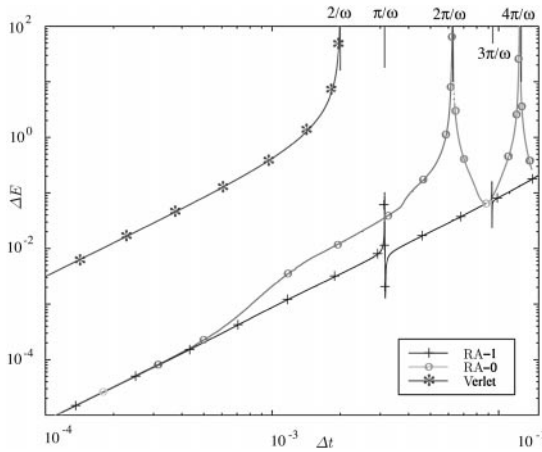

FIG. 7. A log–log scale diagram of the energy error vs step size summarizes improvements from the RA scheme.

Both variants of the RA method are substantially more accurate than the Störmer–Verlet method below the stability threshold. We ran experiments for 1600 values of the step size between $\Delta t = 0.0001$ and $\Delta = 0.016$. The resulting maximum energy errors observed were then plotted against the stepsize, in log–log scale (see Fig. 7). In the high-accuracy (small stepsize) regime, the RA method offered substantial improvement over the Störmer–Verlet method. This is a consequence of the fact that the solution includes a large highly oscillatory component, so that the error is dominated by the approximation of the fast mode. Therefore, the $20\times$ step size reduction for the averaging methods translates into a $400\times$ accuracy improvement below the stability threshold. Moreover, the stable long-term energy behavior typically seen for symplectic and time-reversible methods was observed for both the RA-0 method (away from resonances) and the RA-1 method at all step sizes considered.

The RA-0 method ($b = 1, M = 20$) remained bounded for substantially larger step sizes than the Störmer–Verlet method, up to about $\Delta t = 0.00628$, the location of its first step size resonance. When the RA-1 method was used the results were quite different. Both the overall accuracy of the simulation and the stability behavior were vastly improved. Interestingly, if one looks closely in the vicinity $\Delta t = \pi/\omega$, one finds a modest rise in the errors, indicating a lessening of stability associated with the fast eigenvalue crossing.

We next examined the behavior of the numerical methods for data set B, for which the initial energy is confined to the slow modes. Because of the nonlinear nature of the problem, the high-frequency mode is quickly excited in the Verlet method leading to the same instability observed for the excited highly oscillatory initial data. However, very different results are obtained for the interpolated RA-1 method (see Figs. 8a–8c). At first glance, there is no evidence of instability near 0.00314 and only a high resolution in the step size turns up the slight (but smoothly rounded) bump at long step $\Delta t = 0.003138$, and another such bump near $2\pi/\omega$. *However, at none of the steps considered was there any evidence of the secular growth in energy error that would be associated with a step size resonance.*

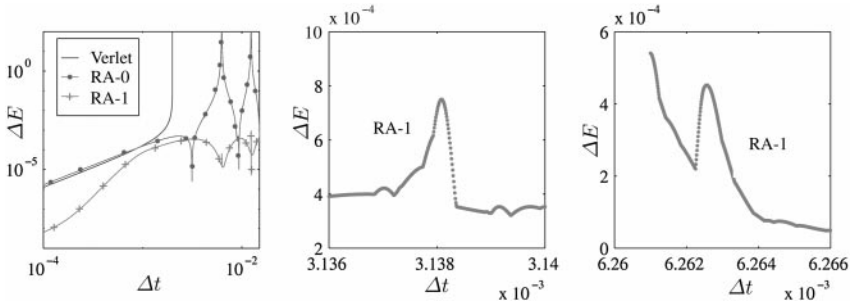

FIG. 8. Efficiency diagram for dataset B. The RA-1 method shows a clear advantage because of the elimination of resonance.

More importantly, there is no evidence of any fast–slow resonance near $2\pi/\omega$, or at any other multiple of π/ω up to the Störmer–Verlet stability threshold. This desirable effect is only observed for the RA-1 method. It was also observed that a substantial improvement in accuracy is obtained from the interpolated averaging method compared with both the Störmer–Verlet and RA-0 methods.

5.1. *Anharmonic Fast Potentials*

The desired effect of the anharmonic potential term is a weakening of resonance effects. It is interesting to ask how far this can be taken when a slight anharmonicity is also present in the fast potential. We further examine the effect of a nonlinearity on the interpolated averaging method (RA-1) by adding a quartic term to the fast potential, viz,

$$V(\boldsymbol{q}, \boldsymbol{\theta}) = \frac{1}{2}(|\boldsymbol{q}|) - 1)^2 + \frac{1}{2}\kappa|\boldsymbol{q} - \boldsymbol{\theta}|^2 + \frac{1}{4}\beta|\boldsymbol{q} - \boldsymbol{\theta}|^4.$$

In our experiment, we chose $\boldsymbol{\pi} = (0.01, 0)$ and took $\beta = 0.1$. For these initial conditions, the slow particle follows very closely the trajectory of the $\beta = 0$ case, while the rapid oscillations of the fast particle are confined to a very narrow range. We again used 20 fast steps per long time step.

Considering first the interval of stepsizes [0.0001, 0.012], we observed very similar behaviors to those obtained without the quartic term. Near each of the three resonance points

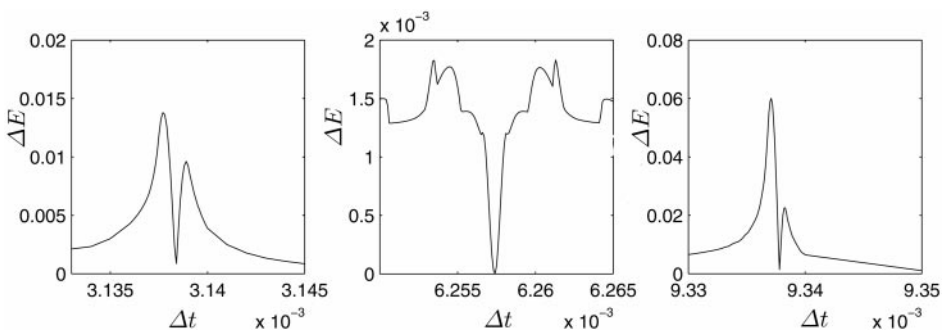

FIG. 9. Energy error vs step size near harmonic resonance points, anharmonic fast potential.

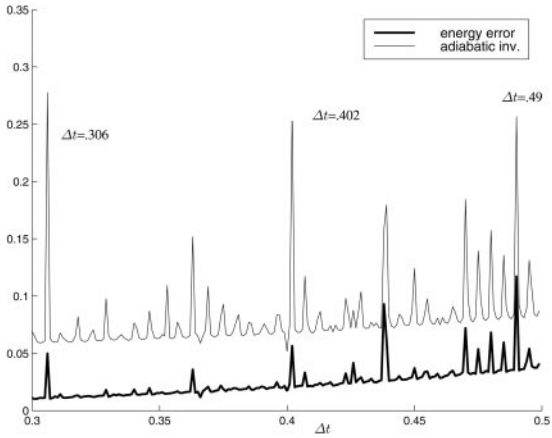

FIG. 10. Very large step size behavior.

($\Delta t = \pi/\omega, 2\pi/\omega$, and $3\pi/\omega$) of the harmonic problem, we see a rise in the amplitude of energy–error variation, but no secular drift in energy (see Fig. 9).

Next we looked at the step size interval [0.012, 0.5]. In general, the method exhibited instability as the small step size used to integrate the fast variables ($\Delta t/M$) crossed the Störmer–Verlet stability boundary, so a large value ($M = 200$, or $M = 400$, depending on the long stepsize) was needed to insure that error in the fast-variable simulation did not seriously affect the results. Remarkably, even in this extremely large step size regime, excellent results were obtained from the averaging method. The energy error is shown in Fig. 10 for 1000 values of Δt between about 0.3 and 0.5. Also shown is the maximum fluctuation in the fast energy adiabatic invariant for each of these runs (the energy error and fast energy fluctuations are roughly correlated).

Trajectories near the linear resonant points—even at the largest peaks of the energy and fast energy fluctuations—are reasonably well resolved. Long simulations (10,000 long time steps) at the worst peaks of the resonance diagram are shown in Fig. 11. Only at the very largest of these steps ($\Delta t = 0.49$) does an unphysical regularity characteristic become evident in the slow dynamics.

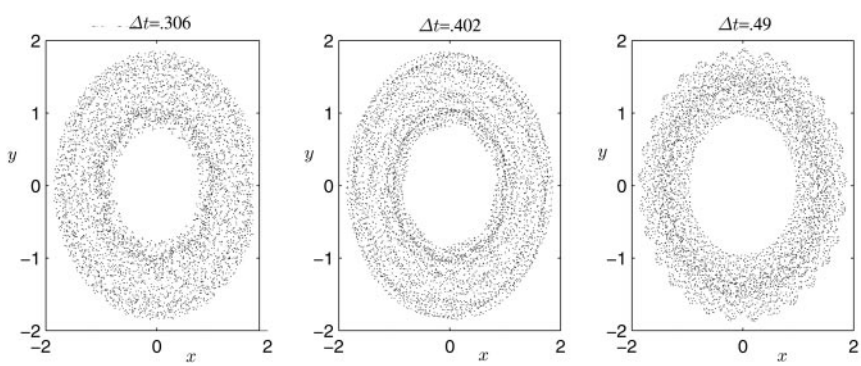

FIG. 11. Very large step size behavior.

6. CONCLUSION

We have presented an averaging integrator for multiple-time-scale dynamics which resolves the fast variables differently than the slow ones. Compared to the Störmer–Verlet method, the new method appears to substantially improve both accuracy and stability behaviors in the large time step (inaccurate) computational domain, although the technique awaits careful evaluation in a challenging application such as molecular dynamics. The observations of this article amply justify such continued study.

APPENDIX A

Methods for Several Fast Variables and Multiple Time Scales

Here we consider a Hamiltonian system with r time scales,

$$\frac{1}{2}\boldsymbol{p}_1^T\boldsymbol{M}_1^{-1}\boldsymbol{p}_1 + \frac{1}{2}\boldsymbol{p}_2^T\boldsymbol{M}_2^{-1}\boldsymbol{p}_2 + \cdots + \frac{1}{2}\boldsymbol{p}_r^T\boldsymbol{M}_r^{-1}\boldsymbol{p}_r + f(\boldsymbol{q}_1, \boldsymbol{q}_2, \ldots, \boldsymbol{q}_r).$$

We assume that the r classes are roughly ordered according to increasing speeds of oscillation. A recursive adaptation of reversible averaging is then possible whereby successive groups of variables are treated with successively smaller time steps.

We will assume the simplest procedure in which the steps decrease geometrically as we treat the faster sets of variables; this is not an essential feature of the scheme. Algorithm 2 demands increasingly more computational work in the faster time scales; this work is consistent with the increasing difficulty of resolving those motions.

ALGORITHM 2 (Reversible Averaging Method for Systems on r Time Scales).

Compute a step of size Δt from given initial values $(\boldsymbol{q}_1^0, \ldots, \boldsymbol{q}_r^0)$ and $(\boldsymbol{p}_1^0, \ldots, \boldsymbol{p}_r^0)$ for the Hamiltonian H.

0. If there is only one fast time scale, apply Algorithm 1.

1. Recursively apply this algorithm for the $r-1$ fast scales (H reduced by freezing $\boldsymbol{q}_1 = \boldsymbol{q}_1^0$), denoting the solutions in the kth time scale by $\boldsymbol{q}_{k,+}(t)$.

2. Slow variable half-step. Average the slowest forces over the fast position values to obtain

$$\bar{\boldsymbol{F}}_{1,+} = -\left\langle \nabla_{\boldsymbol{q}_1} f\left(\boldsymbol{q}_1^0, \boldsymbol{q}_{2,+}(t) \ldots, \boldsymbol{q}_{k,+}(t)\right)\right\rangle,$$

then

$$\boldsymbol{p}_1^{1/2} = \boldsymbol{p}_1^0 + \frac{\Delta t}{2}\bar{\boldsymbol{F}}_{1,+},$$

$$\boldsymbol{q}_1^{1/2} = \boldsymbol{q}_1^0 + \frac{\Delta t}{2}\boldsymbol{M}^{-1}\boldsymbol{p}_1^{1/2}.$$

3. Recursively apply this method to integrate the fast subsystem with H reduced by $\boldsymbol{q}_1 = \hat{\boldsymbol{q}}_1(t)$ (**variant RA-0**: $\hat{\boldsymbol{q}}_1(t) = \boldsymbol{q}_1^{1/2}$; **variant RA-1**: $\hat{\boldsymbol{q}}_1(t) = \boldsymbol{q}_1^0 + \frac{t}{2}\boldsymbol{M}^{-1}\boldsymbol{p}_1^{1/2}$), computing M steps with stepsize $\Delta t/M$, resulting in

$$\boldsymbol{q}_2^1, \boldsymbol{q}_3^1, \ldots, \boldsymbol{q}_r^1,$$

and

$$\boldsymbol{p}_2^1, \boldsymbol{p}_3^1, \ldots, \boldsymbol{p}_r^1.$$

4. Update $\boldsymbol{q}$ to end of step:

$$\boldsymbol{q}_1^1 = \boldsymbol{q}_1^{1/2} + \frac{1}{2}\Delta t \boldsymbol{M}^{-1}\boldsymbol{p}_1^{1/2}.$$

5. This step is analogous to Step 1, but we start with initial values for the fast variables at the right endpoint of the step, and step back in time, again using this method.

6. Compute the averaged slow force $\bar{\boldsymbol{F}}_{1,-}$ and update the slow momentum to end of step:

$$\boldsymbol{p}_1^1 = \boldsymbol{p}_1^{1/2} + \frac{\Delta t}{2}\bar{\boldsymbol{F}}_{1,-}$$

APPENDIX B

Matrix Propagators for RA-0 and RA-1

Let $\mathcal{M}$ represent the propagator for RA-0 and $\mathcal{N}$ the propagator for RA-1. Let A_q, A_θ, A_p, and A_π represent the coefficients of q, θ, p, and π, respectively, in the expression for $p^{1/2}$.

$$A_q = -\frac{1}{2}(\Delta t + \hat{s}), \quad A_\theta = \frac{1}{2}\hat{s}, \quad A_p = 1, \quad A_\pi = \frac{1}{2}(1 - \hat{c}).$$

The matrix $\mathcal{M}$ can be expressed as

$$\mathcal{M} = \begin{bmatrix} 1.0 + \Delta t A_q & \Delta t A_\theta & \Delta t A_p & \Delta t A_\pi \\ (1-\hat{c})\left(1 + \frac{\Delta t}{2} * A_q\right) & \frac{\Delta t}{2}(1-\hat{c})A_\theta + \hat{c} & \frac{\Delta t}{2}(1-\hat{c})A_p & \frac{\Delta t}{2}(1-\hat{c})A_\pi + \hat{s} \\ \mathcal{M}_{31} & \mathcal{M}_{32} & \mathcal{M}_{33} & \mathcal{M}_{34} \\ \hat{s}\left(1 + \frac{\Delta t}{2}A_q\right) & -\hat{s} + \frac{\Delta t}{2}\hat{s}A_\theta & \frac{\Delta t}{2}\hat{s}A_p & \hat{c} + \frac{\Delta t}{2}\hat{s}A_\pi \end{bmatrix},$$

where the third row elements are given in terms of those of the forth row:

$$\mathcal{M}_{31} = A_q - \frac{1}{2}(\Delta t + \hat{s})\mathcal{M}_{11} + \frac{1}{2}\hat{s}\mathcal{M}_{21} - \frac{1}{2}(1-\hat{c})\mathcal{M}_{41},$$

$$\mathcal{M}_{32} = A_\theta - \frac{1}{2}(\Delta t + \hat{s})\mathcal{M}_{12} + \frac{1}{2}\hat{s}\mathcal{M}_{22} - \frac{1}{2}(1-\hat{c})\mathcal{M}_{42},$$

$$\mathcal{M}_{33} = A_p - \frac{1}{2}(\Delta t + \hat{s})\mathcal{M}_{13} + \frac{1}{2}\hat{s}\mathcal{M}_{23} - \frac{1}{2}(1-\hat{c})\mathcal{M}_{43},$$

$$\mathcal{M}_{34} = A_\pi - \frac{1}{2}(\Delta t + \hat{s})\mathcal{M}_{14} + \frac{1}{2}\hat{s}\mathcal{M}_{24} - \frac{1}{2}(1-\hat{c})\mathcal{M}_{44}.$$

The matrix $\mathcal{N}$ can be expressed as

$$\mathcal{N} = \begin{bmatrix} 1.0 + \Delta t A_q & \Delta t A_\theta & \Delta t A_p & \Delta t A_\pi \\ 1 - \hat{c} + (\Delta t - \hat{s}/\omega) * A_q & \hat{c} + (\Delta t - \hat{s}/\omega) * A_\theta & (\Delta t - \hat{s}/\omega)A_p & \hat{s} + (\Delta t - \hat{s}/\omega)A_\pi \\ \mathcal{N}_{31} & \mathcal{N}_{32} & \mathcal{N}_{33} & \mathcal{N}_{34} \\ \hat{s} + (1-\hat{c})A_q/\omega & -\hat{s} + (1-\hat{c})A_\theta/\omega & (1-\hat{c})A_p/\omega & \hat{c} + (1-\hat{c})A_\pi/\omega \end{bmatrix},$$

where the third row elements are given in terms of those of the forth row:

$$\mathcal{N}_{31} = A_q - \frac{1}{2}(\Delta t + \hat{s})\mathcal{N}_{11} + \frac{1}{2}\hat{s}\mathcal{N}_{21} - \frac{1}{2}(1-\hat{c})\mathcal{N}_{41},$$

$$\mathcal{N}_{32} = A_\theta - \frac{1}{2}(\Delta t + \hat{s})\mathcal{N}_{12} + \frac{1}{2}\hat{s}\mathcal{N}_{22} - \frac{1}{2}(1-\hat{c})\mathcal{N}_{42},$$

$$\mathcal{N}_{33} = A_p - \frac{1}{2}(\Delta t + \hat{s})\mathcal{N}_{13} + \frac{1}{2}\hat{s}\mathcal{N}_{23} - \frac{1}{2}(1-\hat{c})\mathcal{N}_{43},$$

$$\mathcal{N}_{34} = A_\pi - \frac{1}{2}(\Delta t + \hat{s})\mathcal{N}_{14} + \frac{1}{2}\hat{s}\mathcal{N}_{24} - \frac{1}{2}(1-\hat{c})\mathcal{N}_{44}.$$

REFERENCES

1. V. I. Arnold, *Mathematical Methods of Classical Mechanics* (Springer-Verlag, New York, 1989).
2. B. García-Archilla, J. M. Sanz-Serna, and R. D. Skeel, Long-time-step methods for oscillatory differential equations, *SIAM J. Sci. Comput.* **20**, 930 (1998).
3. E. Hairer, S. P. Norsett, and G. Wanner, *Solving Ordinary Differential Equations*, I, 2nd ed. (Springer-Verlag, New York, 1994).
4. M. Hochbruck and C. Lubich, A bunch of time integrators for quantum/classical molecular dynamics, in *Computational Molecular Dynamics: Challenges, Methods, Ideas* edited by P. Deuflhard, J. Hermans, B. Leimkuhler, A. Mark, S. Reich, and R. Skeel, Lecture Notes in Computational Science and Engineering. (Springer-Verlag, Berlin, 1999), Vol. 4, p. 421.
5. Marlis Hochbruck, Christian Lubich, A Gautschi-type method for oscillatory second-order differential equations, *Numer. Math.* **83**, 403 (1999).
6. J. S. W. Lamb and J. A. G. Roberts, Time-reversal symmetry in dynamical systems: A survey, *Physica D* **112**, 1 (1998).
7. B. Leimkuhler, S. Reich, and R. D. Skeel, Integration methods for molecular dynamics, in *Mathematical Approaches to Biomolecular Structure and Dynamics*, edited by J. P. Mesirov, K. Schulten, and D. W. Summers, IMA Volumes in Mathematics and its Applications (Springer-Verlag, New York, 1995), Vol. 82.
8. P. Nettesheim and S. Reich, Symplectic multiple-time-stepping integrators for quantum–classical molecular dynamics, in *Lecture Notes in Computational Science and Engineering* (Springer-Verlag, New York, 1998), Vol. 4, p. 412.
9. S. Reich, Multiple time-scales in classical and quantum–classical molecular dynamics. *J. Comput. Phys.* **151**, 49 (1999).
10. R. D. Skeel and J. J. Biesidecki, Symplectic integration with variable stepsize, *Ann. Numer.* Math. **1**, 191 (1994).
11. F. H. Stillinger and C. W. David, Polarization model for water and its ionic dissociation products, *J. Chem. Phys.* **69**, 1473 (1978).
12. M. E. Tuckermann, B. J. Berne, and G. J. Martyna, Reversible multiple time scale molecular dynamics, *J. Chem. Phys.* **97**, 1990 (1993).